Emergent Materials (2022) 5:1109–1116
https://doi.org/10.1007/s42247-021-00281-8

ORIGINAL ARTICLE

Structural morphological and electrical analysis of Pr- And La-doped magnesium ferrites

Muhammad Zeeshan Khan[1] · Shah Zaman[1] · Muhammad Arshad Shehzad Hassan[1] · Asim Khan[1]

Received: 18 June 2021 / Accepted: 21 July 2021 / Published online: 4 August 2021

Abstract

A series of lanthanum and praseodymium incorporated magnesium zinc $Mg_{0.5}Zn_{0.5}Fe_{0.95}Pr_{0.05-x}La_{xO4}$ (x = 0, 0.01, 0.02, 0.03, 0.04) was synthesized by the co-precipitation technique. The sintered and filtered material was characterized by scanning electron microscope (SEM), Fourier transform infrared spectroscopy (FTIR), and UV spectroscopy. The variation in Volume Resistivity and I-V characterizations is analyzed using the two probe method. The Lattice constant, crystallite size, and X-ray density of the ferrites are determined by X-ray diffraction (XRD), which confirms single-phase formation due to incorporating Pr and La. Moreover, the crystalline size of the material was found in the range of 20~42 nm. The vibrational properties were observed by the FTIR spectra analysis that was useful in finding the octahedral and tetrahedral structure of ferrites. The Ultraviolet-visible spectrum was utilized to find the material's energy bandgap and its dependence upon the substituted material concentration as the bandgap increases with the increasing concentration of La. DC resistivity of the material first increased at 100 °C and then decreased with further increase in temperature was due to electron hopping. Moreover, the material's resistivity increases with the increasing La concentration, due to which these materials are a potential candidate for high resistive application.

Keywords X-Ray diffraction · Scanning electron microscope · Pr- and La-doped · Magnesium ferrites · Pr and La · Doping

1 Introduction

Nanoparticles have a significant impact on the electrical, electronic, and medical fields. Many electronic power devices and medical equipment were manufactured based on nanoparticles [1]. When some particle is broken down to the nanoscale, their energy level does not remain continuous. The electrons get scattered at the boundary, and their electrical and other properties are changed [2]. These properties have a groundbreaking effect in engineering, public health, the food industry, and water treatment [3].

Ferrites nanoparticles were synthesized many times by different preparation methods, and various characterization techniques were applied to the ferrite materials. Other elements were incorporated into ferrites to check the effects of concentration so that the required material would have been synthesized to use in industrial applications. K. Ramarao et al. [4] synthesized six samples of magnesium ferrites with general composition $Mg_{1-x}\ Co_x\ Fe_2O_4$ (x = 0.0, 0.1, 0.15, 0.2, 0.25, 0.3) by substituting the cobalt with the solid-state reaction method. After the particle sample synthesizing, they were characterized by such techniques as X-ray diffraction (XRD), Fourier transforms infrared spectroscopy (FTIR), and DC resistance measurement. By the XRD analysis, the formation of single-phase ferrites and their lattice constants was observed at increasing the cobalt amount. Hongru Yang et al. compared the properties of the $ZnFe_2O_4$ nanoparticle prepared with the different methods [5]. The hollow spheres of $ZnFe_2O_4$ nanoparticles produced with the hydrothermal treatment were more sensitive to the gas ethylene glycol and had higher stability. The sensing property was reached due to its hollow structure, higher specific area, and larger pore size. Rohit Sharma et al. [6] evaluated different properties of cobalt-substituted Mg-Zinc ferrites with general formula $Mg_{0.5}\ Zn_{0.5-x}\ CoxFe_2O_4$ (x = 0, 0.125, 0.250, 0.375, 0.500) by XRD, EDS, FTIR, VSM, and UV spectroscopy techniques. The presence of only cubic ferrite phase was obtained by XRD analysis. The change from superparamagnetic to ferromagnetic ferrite phase was found when x was

✉ Muhammad Zeeshan Khan
zeeshankhanee@cqu.edu.cn

[1] Department of Electrical Engineering & Technology, The University of Faisalabad, Punjab 38000, Pakistan

increased above 0.125. The saturation magnetization was observed to be upgraded. Moreover, the dielectric behavior of the ferrite was also observed by applying various frequency ranges.

Hamid Reza Ebrahimi et al. [7] proclaimed the physical and structural property of nickel zinc ferrites with the general formula $Ni_{0.5}Zn_{0.5}Fe_2O_4$ that was synthesized by co-precipitation method with powder and disk samples. It was observed that the magnetization of the samples was changed with the pressure. Moreover, the magnetization could be increased further by applying pressure on the resultant ferrite. The sensitivity of the samples was obtained by keeping the samples in an isolated box. The different gases, i.e., methanol, chloroform, acetone, and acetonitrile, were injected into the chamber, and the material resistance was measured. The effect of significant resistance change was observed in the ferrite interaction to acetonitrile. A.C. Druc et al. [8] reported that cobalt-doped magnesium ferrites with formula $Mg_{1-x}Co_xFe_2O_4$ (x = 0.00, 0.17, 0.34, 0.50, 0.67, 0.84, and 1.00) were produced by sol-gel method. Different techniques were carried out to analyze the structural and physical property of the resultant ferrites samples. The FTIR technique resulted in the deficiency of nitrate groups and organic compound phases. The XRD measurements of the synthesized ferrites verified the single-phase formation. The scanning electron microscope (SEM) technique observed the nanosize ferrite particles. All the produced samples were observed to be immune to electric current.

In this paper, a series of lanthanum and praseodymium incorporated magnesium zinc ferrite with formula $Mg_{0.5}Zn_{0.5}Fe_{0.95}Pr_{0.05-x}$ La_{xO4} at x = 0, 0.01, 0.02, 0.03, and 0.04 was synthesized by the co-precipitation technique. Series of lanthanum and praseodymium incorporated magnesium zinc ferrite with formula $Mg_{0.5}Zn_{0.5}Fe_{0.95}Pr_{0.05-x}La_xO_4$ were designated as S_x, where x = 0, 0.01, 0.02, 0.03, and 0.04 indicates the La contents. The materials were characterized by X-ray diffraction (XRD), Fourier transform infrared spectroscopy (FTIR), and UV spectroscopy. Moreover, the DC bulk resistivity, porosity, and I-V characteristics of Pr- and La-doped magnesium ferrites were measured at different concentrations.

2 Experimental procedure

Pr- and La-doped magnesium ferrites with general formula $Mg_{0.5}Zn_{0.5}Fe_{0.95}Pr_{0.05-x}$ La_{xO4} at x = 0, 0.01, 0.02, 0.03, and 0.04 were synthesized by co-precipitation. The listed materials used in this process are stated below:

$Mg(NO_3)_2.6H_2O$ of 256.41 g/mole
$Zn(NO_3)_2.6H_2O$ of 297.47 g/mole
$Pr(NO_3)_2.6H_2O$ of 435.01 g/mole
$Fe(NO_3)_2.9H_2O$ of 404 g/mole
$La(NO_3)_2.6H_2O$ of 324.92 g/mole

3 Synthesis of material

The starting reagents were weighed according to the stoichiometric ratio. All the samples were poured into the beaker with 100 ml deionized water. All the six samples were then passed through a magnetic stirring process at 80 °C. The PH of the samples was maintained at around 12. Noah's aqueous solution is introduced in the sample to bring its Ph level to 12 by retaining temperatures between 80 °C. After magnetic stirring, all six samples were put on the pre-heated water bath for 12 h. The temperature of the water bath was maintained at 80 °C. The beaker was brought out from the pre-heated water bath after 12 h for the filtration process. The sample's aqueous solution was then dropped on filter paper drop by drop so that all the sample is filtered out, while the water gets down from the filter paper.

Ionized water was spilled into the filter paper in small quantities, and the material was gathered to change the Ph to 7. After reducing Ph, all the samples were washed with ethanol. Materials were kept in the oven at 90 °C for about 70 h. Mortar and pestle is washed adequately with deionized water.

The material was grinded for about 1 h per sample to pulverize it properly. After grinding, all the samples were put in the respective crucible, and the material was converted into fine powder-shaped material. This material was placed in crucibles and kept in the furnace at 850 °C for about 6 h. After getting samples from the furnace, the material was grinded in pestle and mortar until a fine powder was prepared.

4 Characterization techniques

The X-ray diffraction of the materials was used be examine the size of the material and the lattice constant, and X-ray density was calculated w.r.t to miller indices. SEM (Mira T Scan) was used to check the morphology of the material. The FTIR spectra (Alpha, Bruker) were used to analyze the absorption spectra w.r.t and the wavelength of the samples. In addition, Tauc's plot calculated the energy bandgap of the material by using UV characterization. I-V characterization was performed using two probe methods and resistivity behavior of the material w.r.t temperature. A Keithley 8009 resistivity test fixture was used to obtain surface resistivity values at ambient temperature (25 °C).

5 Result and discussion

5.1 X-ray diffraction

The diffraction peak in Fig. 1 at 221, 311, 400, 422, and 511 confirms that the structure is spinel in nature. They dominated the spinel phase at 2θ = 32° and 47 °and indicate secondary phase presence due to the incorporation of $PrFe0_3$. At 2θ = 32°, a reflection peak is observed, indicating that the Pr ions have a meager solubility limit that will decrease the magnesium ferrites' stable reaction. Pr ions are also incorporated with La ions to make secondary phase, and these ions are accumulated on grain boundaries [8]. They also form an insulation layer all around the edges of the grain. The large radii of Pr ions occupy octahedral sites. The size of the crystal is calculated by Scherer's formula, which is stated as follows:

$$D = K\lambda/(\beta \cos \theta) \quad (1)$$

The size of the crystal lies between 20.59 and 41.89 nm. The crystalline size has an abnormal behavior as the Pr and La concentration increases and decreases simultaneously with La concentration. The value of the lattice constant mentioned in the Table 1 depends upon the concentration of Pr^{3+} ions. The constant lattice decreases with the decrease in the concentration of Pr^{3+} ions. The direct relation of Pr^{3+} ions with a lattice constant is due to the larger ionic radius of La^{3+} ions. The ionic radii of Fe^{3+} (= 0.64 A) ions are smaller than that of Pr^{3+} (= 1.13 A), due to which expansion in spinel lattice occurs, causing increases in the lattice constant. The constant lattice decreases as the concentration of Pr^{3+} ions decreases until the value of x = 0.02. It also shows increasing behavior with the rising value of x, which reduces the concentration of $Pr^{3+}$and increases the concentration of La^{3+}. X-ray density of the samples increases at the start with the increasing value of x until x = 0.02. It shows a decreasing trend as the value of x increases, as shown in Table 1. 3D analysis of all the material is shown in Fig. 2. Moreover, the concentration of the La^{3+} ions diffuses in the grain boundaries of the material that ultimately forms an ultra-thin layer, and thus, the constant lattice decreases.

Table 1 Cumulative XRD analysis of Pr and La Doped Magnesium ferrite

Doping concentration	Lattice constant	Crystalline size (nm)	X-ray density
S_0	8.39968	41.89065	3.78743
$S_{0.01}$	8.39587	35.91757	3.79231
$S_{0.02}$	8.36225	39.33482	3.83796
$S_{0.03}$	8.40929	20.59493	3.77361
$S_{0.04}$	8.41303	34.04295	3.76829

Figure 3 shows a plot of porosity versus Pr and La magnesium ferrites. After incorporation of Pr and La, it was observed in decreasing porosity from 16 to 11%. This occurrence may be due to Pr and La ion diffusion during the sintering process into the grain boundaries that result in forming an ultra-thin layer around the grains. Moreover, the segregation process decreases the displacement of grain boundaries and further reduces crystal growth.

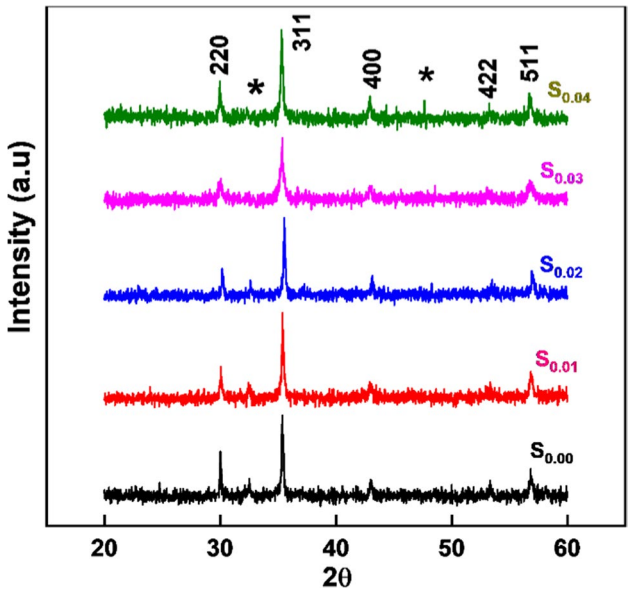

Fig. 1 XRD analysis of Pr- and La-doped magnesium ferrites

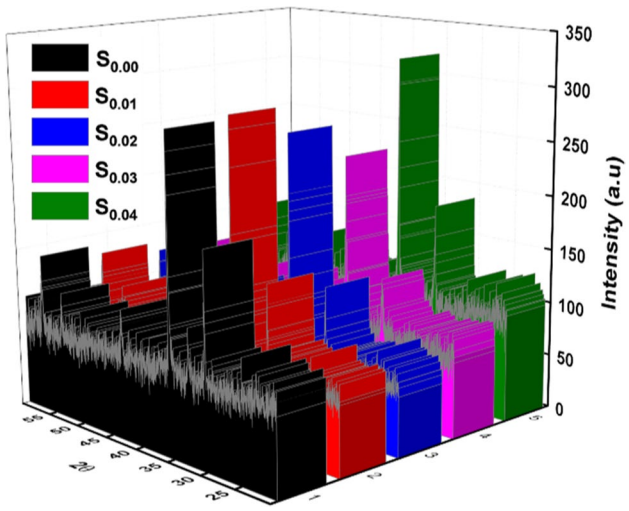

Fig. 2 3D XRD analysis of Pr- and La-doped magnesium ferrites

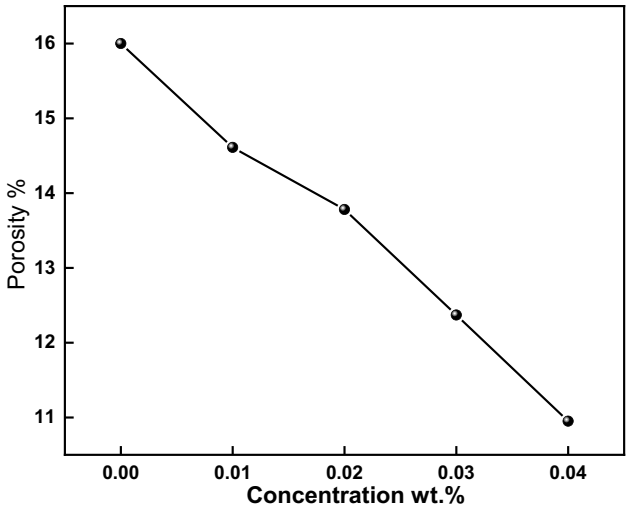

Fig. 3 Porosity versus Pr- and La-doped magnesium ferrites

5.2 Morphological analysis

SEM images of La- and Pr-doped magnesium ferrites are shown in Fig. 4. It was observed that the particle size is somewhat dependent upon the dopant that is introduced in the magnesium ferrites. The sample exhibits irregular shape and size. There are no clear boundaries due to the secondary phase after incorporation of La and Pr. Moreover, the rare earth materials occupy the grain boundaries or the ions' positions as the tetrahedral sites are too small to be occupied by an area of Fe^{3+} [9]. Here, with the increasing value of x, the concentration of Pr decreases, while the concentration of La increases, resulting in the crystal's irregular size as the grain size decreases with the increasing concentration of Pr ions [10]. It was observed that grains of all the samples are agglomerated due to rare earth materials doping. Rare earth doping in the ferrites can cause inconsistencies in the material confirmed by the XRD result.

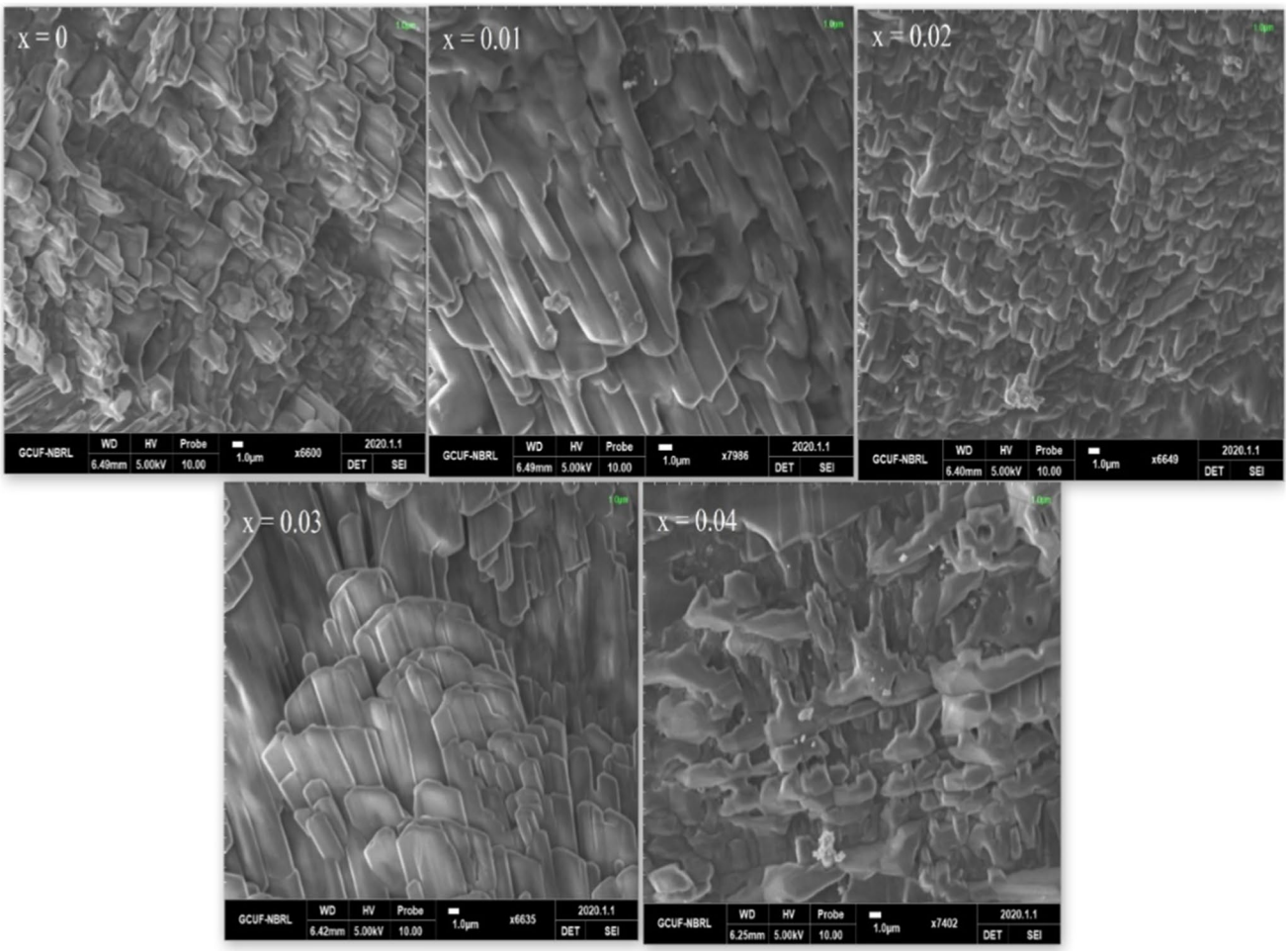

Fig. 4 Surface morphological analysis of Pr- and La-doped magnesium ferrites

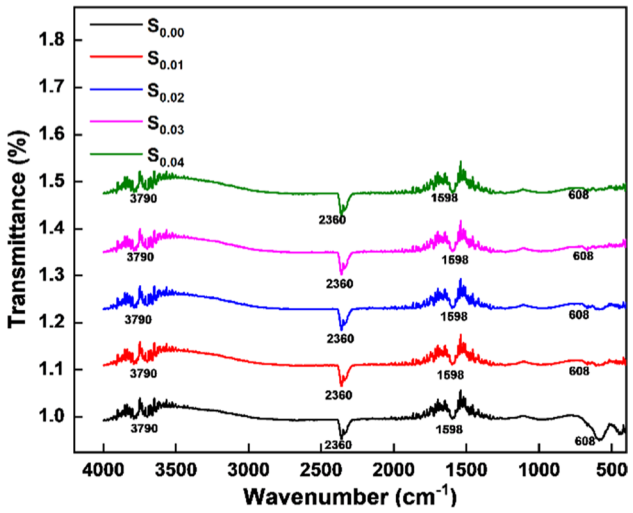

Fig. 5 FTIR of Pr- and La-doped magnesium ferrites

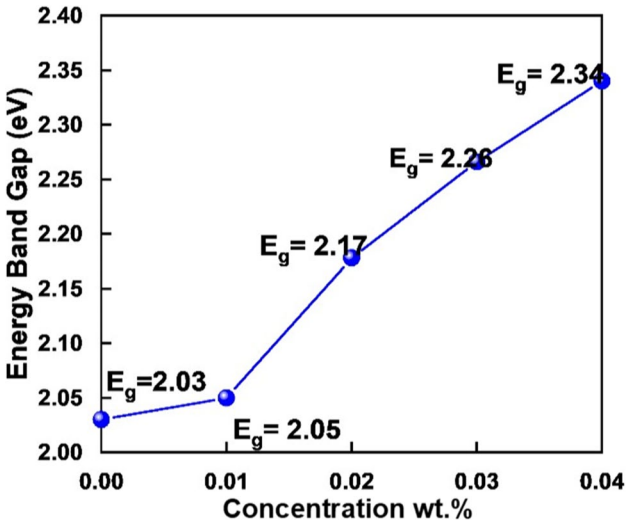

Fig. 7 Cumulative analysis energy bandgap of Pr- and La-doped magnesium ferrites

5.2.1 FTIR

FTIR spectra of the synthesized material were recorded in 400–4000 cm^{-1} at room temperature. The recorded spectra revealed the characteristics and absorption peaks of ferrites. Moreover, the node of the tetrahedral and octahedral structure of ferrites was also observed. The cumulative analysis of all the samples is shown in Fig. 5. CO bonding spectrum was observed at around 3790 cm^{-1} for all the samples showing absorption in the material due to moisture in the environment. The range observed at 2360 cm^{-1} for all the samples was mainly due to O=H bonding originating from the atmosphere. One more spectrum examined for all the samples at 1598 cm^{-1} was primarily due to absorption(C-O). The tetrahedral symmetry was observed for all the samples at 608 cm^{-1}, indicating the structure of ferrites.

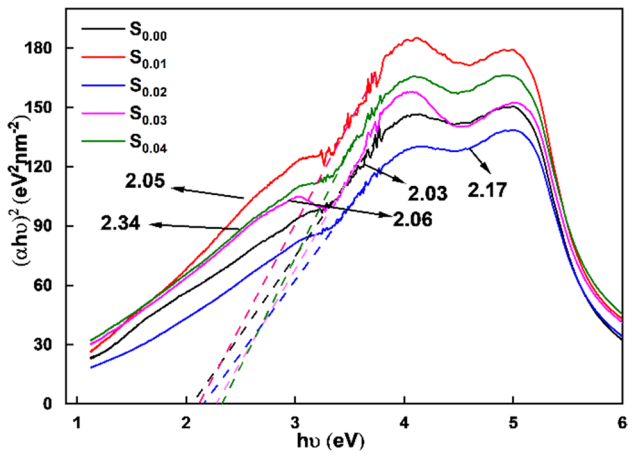

Fig. 6 Tauc's plot of Pr- and La-doped magnesium ferrites

5.3 UV spectroscopy analysis

The UV-visible spectrum investigated La- and praseodymium (Pr)-substituted magnesium ferrite's optical properties. The spectra of Pr- and La-substituted ferrites were seen in the spectral range of 300–900 nm, respectively, at concentration x = 0, indicating that the spectrum lies in the visible region. It was also observed that the absorption spectrum decreased with the increase in wavelength. Moreover, in pure magnesium ferrites $MgFe_2O_4$ samples, absorption percentage decreases with increasing calcination temperature. Pr's substitution was due to the densification of the samples' overall structure with the increase in calcination temperature. A cumulative analysis of the energy bandgap is performed by plotting all the samples' energy bandgap values at various concentrations by using Tauc's plot shown in Fig. 6 and cumulative energy and gap analysis in Fig. 7. The energy bandgap increases with the rising concentration of La^{3+}, while the concentration of Pr^{3+} decreases simultaneously, as shown in Table 2. This occurrence can be explained due to the following reasons. The direct bandgap variation may be due to the low electron momentum observed on the energy bandgap [11]. The material has an average bandgap

Table 2 Pr- and La-doped magnesium ferrite at various concentration versus energy bandgap

Doping concentration	Energy Bandgap
S_0	2.03
$S_{0.01}$	2.05
$S_{0.02}$	2.17
$S_{0.03}$	2.26
$S_{0.04}$	2.34

value of 2.22 eV. Furthermore, Pr- and La-doped magnesium ferrites' bandgap was in the range of 2.03–2.38 eV and shows an increasing trend after incorporating the La^{3+} as it exhibits high resistive property. The more the concentration of La^{3+} ions, the more the bandgap energy required the optical band to shift towards a higher energy band.

5.4 DC volume resistivity

The DC volume resistivity of ferrites with Pr- and La-doped magnesium ferrites at various temperatures was performed. Magnesium- and zinc-substituted ferrites are composed of grain and grain boundaries, while grains exhibit conductive properties compared to the grain boundaries that make ferrites a conductive material.

The DC resistivity of the material is calculated with different concentrations of the Pr^{3+}. The resistivity of material gets increased with the concentration of the Pr^{3+} ions as Pr^{3+} significantly affects the grain boundaries, which has a valuable role in the material's resistivity [12], as shown in Fig. 8. With the increasing value of x, the concentration of La^{3+} increases, while the concentration of Pr^{3+} decreases. With the temperature increment, the mobility of the charge carrier's changes may lead to the hopping of one La^{3+} atom to the other La^{3+} atom that increases the conduction. The presence of La^{3+} only obstructs hopping between the tetrahedral sites. Also, the hopping of conductive electrons between trivalent and divalent ferrite ions at octahedral sites enhances conduction in materials [13]. The material's resistivity increases as the concentration of rare earth material such as Pr and La increases [14]. The DC resistivity also depends upon the temperature of the material. As the material's temperature rises, the DC resistivity of the material also increases until it reaches up to a temperature range of 85 to 100 °C, and then it decreases drastically at 330 °C. Moreover, all the materials' resistivity remains constant until the temperature reaches 460 °C [15]. It can be concluded that these materials exhibit high resistivity for substituted soft ferrites, which have larger ionic radii [16]. Moreover, during the slow cooling of the material, the oxidation of La^{3+} ions inside the grain boundaries gets impeded due to the formation of an insulating layer that significantly increases the material's resistivity [17].

The resistivity increases may also be due to increased porosity, hindering the charge carrier's motion, resulting in resistivity [18]. The sample's semiconductor behavior can be seen as above a specific temperature, the resistivity of the material decreases, which follows the Arrhenius equation [19]. Pr^{3+} ions usually prefer to occupy the octahedral site due to the conversion of some La^{3+} ions to the tetrahedral site. This would limit the hopping and thus increases the resistivity too.

5.5 Current-voltage characteristics

Figure 9 shows a typical current-voltage behavior at 40 °C of Pr- and La-doped magnesium ferrite at x = 0, 0.01, 0.02, 0.03, and 0.04. It can be observed that for all the samples, Ohmic behavior was observed. Also, the current-voltage behavior of any material at low temperature is linear due to thermally generated carriers. The presence of grain boundaries layers can explain the Ohmic behavior due to which the conduction in the material does not occur. There is a very little change in the current w.r.t the voltage at x = 0 due to La ions' concentration, which occupies the grain boundaries, and a very little change in the current was obvious. According to the solid band structure, an insulator consists of a full valance bond separated

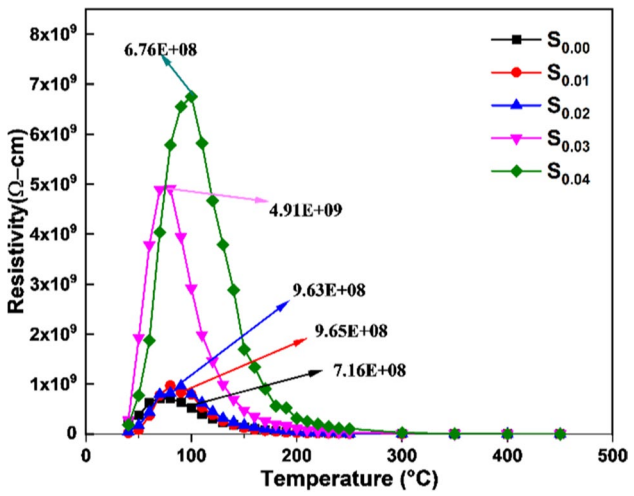

Fig. 8 Resistivity versus temperature of Pr- and La-doped magnesium ferrites

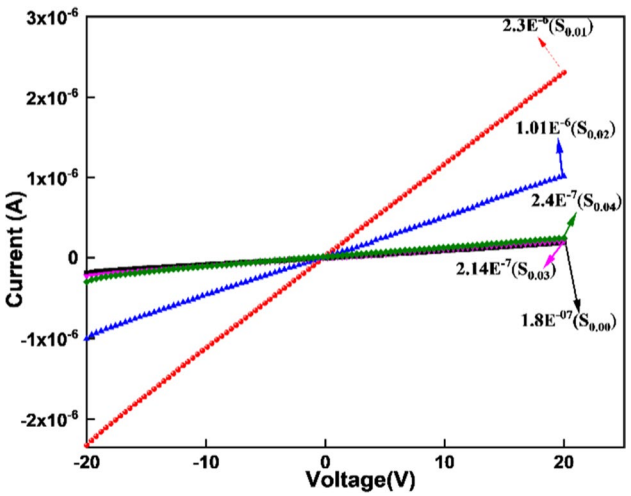

Fig. 9 I-V behavior of Pr- and La-doped magnesium ferrites at 40 °C

by an empty conduction band with a maximum energy bandgap. Conduction cannot occur in the empty band until and unless additional carriers in the conduction are introduced. Carrier may be injected from any metal electrode or metal-insulator electrode. A space charge is built up in material after incorporating La^{3+} and Pr^{3+}, resulting in material conduction due to electron hopping [20–22]. The above analysis confirmed that the material's resistivity gets increased with the concentration of La^{3+} ions, due to which conduction also decreased. Ferrites are semiconductors whose resistivity decreases as the temperature increases that may result in rising the current.

6 Conclusion

Pr- and La-doped magnesium ferrites were synthesized effectively through the co-precipitation method to analyze the structure morphology, crystalline size, XRD, energy bandgap, and lattice constant. X-ray diffraction confirms the structure as a single-phase structure with a secondary phase due to the concentration of Pr^{3+} and La^{3+}. Moreover, XRD shows an increasing trend at concentration, i.e., $x = 0$ to 0.02, and then decreases drastically from $x = 0.03$ to 0.04. This occurrence can be due to the structural property's variation and dependence on Pr^{3+} and La^{3+} doping and distribution concentration. From SEM analysis, it was observed that the sample exhibits irregular shape and size. There were no clear boundaries due to the secondary phase after incorporation of La and Pr. Fourier transform infrared spectroscopy (FTIR) was employed for Pr- and La-doped magnesium ferrites' chemical characterization. The characteristics of ferrites, oxygen-metal structure, the tetrahedral node, and octahedral structure were obvious after incorporating Pr3+ and La3+ ions at various concentrations. The energy bandgap of the material shows dependency on Pr^{3+} and La^{3+} ions as the energy bandgap increases with the rising concentration of La^{3+}, while the concentration of Pr^{3+} decreases simultaneously; low electron momentum is obvious in the energy bandgap. The material's electrical characteristics such as I-V and volume resistivity show dependency upon La and Pr ions' concentration. Moreover, resistivity increases with the concentration of La^{3+} due to electron hopping, making this material significant for higher temperature application.

Acknowledgements This research was carried out in collaboration with the Department of Physics, Government College University Faisalabad Pakistan.

Declarations

Conflict of interest The authors declare no competing interests.

References

1. Y. Yang, A. Chawla, J. Zhang, A. Esa, H.L. Jang, & A. Khademhosseini, Applications of nanotechnology for regenerative medicine; healing tissues at the nanoscale. in principles of regenerative medicine. Academic Press. 485–504 (2019). https://doi.org/10.1016/B978-0-12-809880-6.00029-1
2. J. Mathew, J. Joy, & S.C. George, Potential applications of nanotechnology in transportation: a review. J. of King Saud Uni. Sci. **9**, 586–594 (2019). https://doi.org/10.1016/j.jksus.2018.03.015
3. M. Z. Khan, F. Wang, Li He, Z. Shen, Z. Huang and M. A. Mehmood, Influence of treated nano-alumina and gas-phase fluorination on the dielectric properties of epoxy resin / alumina nanocomposites. IEEE Trans. Dielectr. Electr. Insul. **27**, 410–417 (2020). https://doi.org/10.1109/TDEI.2019.008392
4. K. Ramarao, B.R. Babu, B.K. Babu, V. Veeraiah, S.D. Ramarao, K. Rajasekhar, A.V. Rao, Composition dependence of structural, magnetic and electrical properties of Co substituted magnesium ferrite. Phys. B: Cond. Matter **528**, 18–23 (2018). https://doi.org/10.1016/j.physb.2017.10.072
5. H. Yang, X. Bai, P. Hao, J. Tian, Y. Bo, X. Wang, H. Liu, A simple gas sensor based on zinc ferrite hollow spheres: highly sensitivity, excellent selectivity and long-term stability. Sen. and Actu. B: Chemical **280**, 34–40 (2019). https://doi.org/10.1016/j.snb.2018.10.056
6. R. Sharma, P. Thakur, M. Kumar, N. Thakur, N.S. Negi, P. Sharma, V. Sharma, Improvement in magnetic behaviour of cobalt doped magnesium zinc nano-ferrites via co-precipitation route. J. of Alloys and Compounds **684**, 569–581 (2016). https://doi.org/10.1016/j.jallcom.2016.05.200
7. H. R. Ebrahimi, M. Parish, G. R. Amiri, B. Bahraminejad, & S. Fatahian, Synthesis, characterization and gas sensitivity investigation of Ni0. 5Zn0. 5Fe_2O_4 nanoparticles. J. of Magnetism and Magnetic Mater. **414**, 55–58 (2016). https://doi.org/10.1016/j.jmmm.2016.04.043
8. A. Vasiliu, Gh. Maxim, M. L. Craus, E. Luca, "Some magnetic properties and the phase equilibrium of the compounds in the CaxNi1–xFe_2O_4 system Physica status solidi (a), 371–376 (1972). https://doi.org/10.1002/pssa.2210130204
9. M.Z. Said, Effect of gadolinium substitutions on the structure and electrical conductivity of Ni-ferrite. Mater. Letters **34**, 305–307 (1998). https://doi.org/10.1016/S0167-577X(97)00201-2
10. M.T. Farid, I. Ahmad, M. Kanwal, G. Murtaza, I. Ali & S. A Khan, S. A. The role of praseodymium substituted ions on electrical and magnetic properties of Mg spinel ferrites. J. of Magnetism and Magnetic Materials, **428**, 136–143 (2017). https://doi.org/10.1016/j.jmmm.2016.12.031
11. P.P. Hankare, S.D. Jadhav, U.B. Sankpal, R.P. Patil, R. Sasikala, I.S. Mulla, Gas sensing properties of magnesium ferrite prepared by co-precipitation method. J. of Alloys and Compounds **488**, 270–272 (2009). https://doi.org/10.1016/j.jallcom.2009.08.103
12. M.R. Eraky, S.M. Attia, Transport properties of Ti–Ni spinel ferrites. Physica B: Condensed Matter **462**, 97–103 (2015). https://doi.org/10.1016/j.physb.2015.01.011
13. E. Rezlescu, N. Rezlescu, P.D. Popa, L. Rezlescu, & C. Pasnicu, The influence of R_2O_3 (R= Yb, Er, Dy, Tb, Gd, Sm and Ce) on the electric and mechanical properties of a nickel–zinc ferrite. physica status solidi (a), **162**, 673–678 (1997). https://doi.org/10.1002/1521-396X(199708)162:2<673::AID-PSSA673>3.0.CO;2-A
14. S.E. Jacobo, S. Duhalde, H.R. Bertorello, Rare earth influence on the structural and magnetic properties of NiZn ferrites. J. of Magnetism and Magnetic Materials **272**, 2253–2254 (2004). https://doi.org/10.1016/j.jmmm.2003.12.564
15. U. Ghazanfar, S.A. Siddiqi, G. Abbas, Study of room temperature dc resistivity in comparison with activation energy and drift

mobility of NiZn ferrites. Mater. Sci. and Eng. B **118**, 132–134 (2005). https://doi.org/10.1016/j.mseb.2004.12.086
16. N. Rezlescu, E. Rezlescu, C. Pasnicu, & M. L. Craus, Effects of the rare-earth ions on some properties of a nickel-zinc ferrite. J. of Phy.: Cond. Matter, **29**, 5707 (1994). https://doi.org/10.1088/0953-8984/6/29/013
17. M.J. Iqbal, M.N. Ashiq, Physical and electrical properties of Zr–Cu substituted strontium hexaferrite nanoparticles synthesized by co-precipitation method. Chem. Eng. J. **136**, 383–389 (2008). https://doi.org/10.1016/j.cej.2007.05.046
18. A.A. Sattar, H.M.E. Sayed, K.M. Shokrofy, M.M.E. Tabey, Improvement of the magnetic properties of Mn-Ni-Zn ferrite by the non-magnetic Al-ion substitution. J. Appl. Sci **5**(1), 162–168 (2005). https://doi.org/10.1016/j.jare.2013.08.005
19. I. Ahmad, M.T. Farid, R. Kousar, S.B. Niazi, Structural and electrical properties of lanthanum substituted spinel ferrites. World Appl. Sci. J. **22**, 796–801 (2013). https://doi.org/10.5829/idosi.wasj.2013.22.06.281
20. J. Jung, D. Bae, S. Kim, H.D. Kim, Self-rectifying resistive switching phenomena observed in Ti/ZrN/Pt/ p -Si structures for crossbar array memory applications. Applied Physics Letters **118**, 112106 (2021). https://doi.org/10.1063/5.0036528
21. K.H. Kim, M.J. Yun, S. Kim, H.D. Kim, Improved contact properties of single-walled carbon nanotube on p-AlGaN layers after microwave post-treatment. J. of Chem. and Phys. **252**, 123471 (2020). https://doi.org/10.1016/j.matchemphys.2020.123471
22. M. Ju Yun, S. Kim, S. Kim and H.-D. Kim, Memory state protected from leakage current in Ti/SiN/NiN/Pt bilayer resistive random-access memory devices for array applications, Journal of Nanoscience and Nanotechnology, Semicond. Sci. Technol. **34**, 075030 (2019). https://doi.org/10.1088/1361-6641/ab2324